Copper(I) *tert*-Butylthiolato Clusters as Single-Source Precursors for High-Quality Chalcocite Thin Films: Precursor Chemistry in Solution and the Solid State

Sven Schneider,[†,‡] Alma Dzudza,[†] Gabriele Raudaschl-Sieber,[‡] and Tobin J. Marks*[,†]

Department of Chemistry, Materials Research Center, and Department of Materials Science and Engineering, Northwestern University, Evanston, Illinois 60208-3113, and Technische Universität München, Lichtenbergstrasse 4, 85747 Garching, Germany

Received January 7, 2007

Polymeric $(CuS^tBu)_\infty$ (**1**) undergoes reaction with trialkylphosphines to form the cuprous thiolato phosphine complexes $[(CuS^tBu)_4(PR_3)_2]$ (R = Me (**2a**), Et (**2b**)) in high yield. In contrast to **2b**, in polar solvents (CH_2Cl_2, tetrahydrofuran), complex **2a** is in equilibrium with the ion pair $Cu(PMe_3)_4^+Cu_5(S^tBu)_6^-$ (**3**) and other species such as $(CuS^tBu)_x(PMe_3)_2$ (x = 6 (**4**), 8 (**5**)). Clusters **2**−**4** were isolated analytically pure and fully characterized in solution by multinuclear nuclear magnetic resonance (NMR) spectroscopy and in the solid state by single-crystal X-ray diffraction and ^{31}P magic angle spinning NMR spectroscopy, while the structure of compound **5** was determined by single-crystal X-ray diffraction. Thermal analysis (TGA/DTA) and examination of the volatile byproducts suggest stepwise phosphine loss and C−S bond cleavage by isobutene elimination as the predominant thermolysis pathways of this new Cu_2S precursor class.

Introduction

Copper thiolates are of great current interest because of their photochemical properties,[1] their relevance to metallothionein proteins,[2] and their utility as organocuprate synthetic reagents.[3] In the last several years, mixed metal copper(I) thiolates have been successfully employed as *single-source* precursors for chalcopyrite ($CuMS_2$, M = Ga, In) thin films and nanoparticles for photovoltaics (PV).[4] Although thiols have been used as the sulfur source for the preparation of binary Cu_2S nanoparticles, effective cuprous thiolate *single-source* precursors for Cu_2S growth remain elusive.[5]

Neutral, binary copper(I) thiolates CuSR (e.g., R = Me, Et, ^{n}Pr, ^{i}Pr, ^{n}Bu, ^{t}Bu, Ph) are potential Cu_2S precursor candidates but are generally insoluble in most organic solvents and considered to be coordination polymers. Only the structure of the polymeric parent alkylthiolate $(CuSMe)_\infty$, derived from powder diffraction data by Rietveld techniques, has been analyzed,[6] and Dance predicted a similar chain structure for $(CuS^tBu)_\infty$.[7] Except for this work, only a limited number of oligomeric, neutral homoleptic copper(I) complexes having very bulky monodentate thiolate ligands, $[CuSR]_n$ (R = C_6H_2-2,4,6-^{i}Pr$_3$, n = 4, 8; R = C_6H_4-2-SiMe$_3$, n = 12; R = C_6H_3-2,6-(SiMe$_3$)$_2$, n = 4), have been structurally characterized.[8] Consequently, homoleptic copper(I) thiolates generally lack sufficient volatility to be useful as *single-source* precursors for low-pressure chemical vapor deposition (LP-CVD) of Cu_2S films. Indeed, we find that CuS^tBu (**1**) sublimes at ∼160 °C/10 mTorr but slowly decomposes under these conditions, leading to sintering in the CVD precursor reservoir and therefore unstable mass transport.[9] In contrast, liquid precursor delivery in conjunction with aerosol-based film deposition methods does not require volatile precursors.[10] While the structural chemistry of neutral Cu(I) thiolato triphenylphosphine adducts in the

[†] Northwestern University.
[‡] Technische Universität München.

(1) Yam, V. W.-W.; Lam, C. H.; Fung, W. K.-M.; Cheung, K.-K. *Inorg. Chem.* **2001**, *40*, 3435.
(2) (a) Solomon, E. I.; Randall, D. W.; Glaser, T. *Coord. Chem. Rev.* **2000**, *200*−*202*, 595. (b) Henkel, G.; Krebs, B. *Chem. Rev.* **2004**, *104*, 801.
(3) Janssen, M. D.; Grove, D. M.; van Koten, G. *Prog. Inorg. Chem.* **1997**, *46*, 97.
(4) (a) Hirpo, W.; Dhingra, S.; Sutorik, A. C.; Kanatzidis, M. G. *J. Am. Chem. Soc.* **1993**, *115*, 1597. (b) Hollingsworth, J. A.; Hepp, A. F.; Buhro, W. E. *Chem. Vap. Deposition* **1999**, *5*, 105. (c) Banger, K. K.; Cowen, J.; Hepp, A. F. *Chem. Mater.* **2001**, *13*, 3827. (d) Banger, K. K.; Harris, J. D.; Cowen, J. E.; Hepp, A. F. *Thin Solid Films* **2002**, *403*−*404*, 390. (e) Hollingsworth, J. A.; Banger, K. K.; Jin, M. H.-C.; Harris, J. D.; Cowen, J. E.; Bohannan, E. W.; Switzer, J. A.; Buhro, W. E.; Hepp, A. F. *Thin Solid Films* **2003**, *431*−*432*, 63. (f) Castro, S. L.; Bailey, S. G.; Raffaelle, R. P.; Banger, K. K.; Hepp, A. F. *Chem. Mater.* **2003**, *15*, 3142. (g) Castro, S. L.; Bailey, S. G.; Raffaelle, R. P.; Banger, K. K.; Hepp, A. F. *J. Phys. Chem. B* **2004**, *108*, 12429.
(5) (a) Larsen, T. H.; Sigman, M.; Ghezelbash, A.; Doty, R. C.; Korgel, B. A. *J. Am. Chem. Soc.* **2003**, *125*, 5638. (b) Sigman, M. B., Jr.; Ghezelbash, A.; Hanrath, T.; Saunders, A. E.; Lee, F.; Korgel, B. A. *J. Am. Chem. Soc.* **2003**, *125*, 16050. (c) Chen, L.; Chen, Y.-B.; Wu, L.-M. *J. Am. Chem. Soc.* **2004**, *126*, 16334. (d) Kuzuya, T.; Tai, Y.; Yamamuro, S.; Sumiyama, K. *Sci. Technol. Adv. Mater.* **2005**, *6*, 84.
(6) Baumgartner, M.; Schmalle, H.; Baerlocher, C. *J. Solid State Chem.* **1993**, *107*, 63.
(7) Dance, I. G. *Polyhedron* **1988**, *7*, 2205.
(8) (a) Yang, Q.; Tang, K.; Liao, H; Han, Y.; Chen, Z.; Tang, Y. *J. Chem. Soc., Chem. Commun.* **1987**, 1076. (b) Block, E.; Gernon, M.; Kang, H.; Liu, S.; Zubieta, J. *J. Chem. Soc., Chem. Commun.* **1988**, 1031. (c) Block, E.; Gernon, M.; Kang, H.; Ofori-Okai, G.; Zubieta, J. *Inorg. Chem.* **1989**, *28*, 1263. (d) Block, E.; Kang, H.; Ofori-Okai, G.; Zubieta, J. *Inorg. Chim. Acta.* **1990**, *167*, 147. (e) Schroeter-Schmid, I.; Strähle, J. *Z. Naturforsch., B* **1990**, *45*, 1537.
(9) Schneider, S.; Yang, Y.; Marks, T. J. *Chem. Mater.* **2005**, *17*, 4286.
(10) Choy, K. L. *Prog. Mater. Sci.* **2003**, *48*, 57.

10.1021/cm0700504 CCC: $37.00
Published on Web 04/25/2007

solid state has been previously discussed,[11] no efficient synthetic route for their preparation in high yields has been described, and the solution structural/compositional behavior of curous thiolato phosphine clusters was not examined in detail.

Recently, we described the synthesis and characterization of $(CuS^tBu)_4(PMe_3)_2$ (**2a**), which is readily soluble in organic solvents, and its implementation as the first *single-source* precursor for the α-Cu_2S thin film growth by aerosol-assisted chemical vapor deposition (AACVD).[9] We further reported copper(I) mixed ligand thiolato hexafluoroacetylacetonato (hfa^-) clusters as potential Cu_2S *single-source* precursors and showed that the thermolysis pathways of the thiolate entity can be controlled by the interplay of C−S bond activating Lewis acid and C−S stabilizing Lewis base cluster building blocks.[12] In this contribution we present a full discussion of the synthesis of the trimethyl- and triethylphosphine stabilized *tert*-butylthiolato clusters $Cu(PMe_3)_4^+Cu_5(S^tBu)_6^-$ (**3**) and $(CuS^tBu)_n(PR_3)_2$ (R = Me, n = 4 (**2a**), 6 (**4**), 8 (**5**); R = Et, n = 4 (**2b**)), characterize their structural properties in solution, the solid state, and the gas phase, and investigate the thermolysis of this new class of α-Cu_2S *single-source* precursors.

Experimental Section

Materials and Methods. PMe_3 and PEt_3 were obtained from Aldrich and used without further purification. CuS^tBu (**1**) and $(CuS^tBu)_4(PMe_3)_2$ (**2a**) were synthesized as described earlier.[9] All synthetic manipulations were carried out under an atmosphere of N_2 using standard Schlenk techniques or in a N_2-filled glovebox. Diethyl ether and tetrahydrofuran (THF) were distilled from sodium benzophenone ketyl immediately before use. Pentane and toluene were dried and deoxygenized by passing through columns packed with activated molecular sieves and Q5, respectively.

Analytical Methods. Elemental analyses were performed by the Microanalytical Laboratories of the University of Illinois Urbana−Champaign and the Technische Universität München. Solution NMR spectra were recorded on a VARIAN Mercury 400 spectrometer or a VARIAN Inova 400 spectrometer equipped with a variable-temperature unit, with shifts for ^1H and ^{13}C referenced to the solvent signal (C_6D_6, toluene-d_8, $CDCl_3$, CD_2Cl_2, THF-d_8). The ^{31}P chemical shifts are reported relative to external phosphoric acid (δ 0.0 ppm). For ^{31}P magic angle spinning (MAS) NMR spectroscopy, microcrystalline samples were packed under inert gas into a 4 mm ZrO_2 rotor sealed with a Kel-F cap. The spectra were recorded with a BRUKER Avance 300 spectrometer at 121.5 MHz with high power decoupling (HPDEC) and an MAS frequency of 8 kHz (pulse width 1.5 μs, repetition time 10 s). Chemical shifts are referenced to external $NH_4H_2PO_4$ (δ 1.11 ppm). Assignments of thermolysis products were made by comparison with spectra of original samples (signals in C_6D_6 [ppm]: HS^tBu ^1H δ 1.21 (s, 9H), 1.63 (s, 1H); S^tBu_2 ^1H δ 1.34 (s); $S_2{}^tBu_2$ ^1H δ 1.22 (s); H_2S ^1H δ 0.20 (s); PMe_3 ^1H δ 0.80 (d, $^2J_{HP}$ = 2 Hz); ^{31}P δ −61.8 (s); $SPMe_3$ ^{31}P δ 59.1 (s); PEt_3 ^1H δ 0.97 (dt, $^3J_{HP}$ = 13 Hz, $^3J_{HH}$ = 8 Hz, 3H), 1.21 (q, $^3J_{HH}$ = 8 Hz, 2H); ^{31}P δ −19.1 (s); $SPEt_3$ ^{31}P δ 53.4 (s)) or comparison with literature data (signals in C_6D_6 [ppm]: CH_2CMe_2 ^1H δ 1.60 (t, ^4J = 1 Hz); 4.75 (sept, ^4J = 1 Hz); $HCMe_3$ ^1H δ 0.863 (d, 10 H, ^3J = 7 Hz); 1.64 (dec, 1 H, ^3J = 7 Hz)).[13] Mass spectra were obtained on a Thermo Finnegan LCQ Advantage LC/MS by direct injection of the solution downstream of the column. Thermogravimetric analysis (TGA) data were collected on a TA Instruments model SDT 2960 at atmospheric pressure, with an N_2 flow rate of 100 mL/min and a temperature ramp of 1 °C/min. Volatile thermolysis products were examined (NMR, GC-MS) by heating solid samples (∼200 mg) at atmospheric pressure under a stream of N_2 and sweeping the hot decomposition products into a liquid N_2-cooled trap. GC-MS analysis was performed on a HP6890 gas chromatograph with a quadrupole MS detector with NMR samples in C_6D_6 diluted with CH_2Cl_2.

Syntheses. *$[(CuS^tBu)_4(PEt_3)_2]$ (**2b**).* To a suspension of CuS^tBu (**1**; 6.109 g; 40.00 mmol) in Et_2O (50 mL) was added PEt_3 (2.97 mL, 2.38 g, 20.1 mmol) via a syringe. The starting material dissolved to form a yellow, slightly cloudy solution. After 0.5 h at 25 °C, the solution was filtered, and the solvent evaporated in vacuo until the colorless product began to precipitate. The mixture was then stored at −40 °C overnight. Colorless microcrystals of **3** were collected by filtration, washed twice with 20 mL of Et_2O at −78 °C, and dried in vacuo at 25 °C for 3 h. Yield: 6.691 g (31.59 mmol, 79%). Anal. Calcd for $C_{28}H_{66}Cu_4P_2S_4$ (847.22): C, 39.70; H, 7.85. Found: 39.55; H, 7.92. NMR (C_6D_6, rt, [ppm]) ^1H NMR (400.2 MHz): δ 1.02 (3 H, dt, $^3J_{HH}$ = 7 Hz, $^3J_{PH}$ = 16 Hz, PCH_2CH_3), 1.45 (2 H, m, PCH_2CH_3), 1.74 (6 H, s, CCH_3). ^{13}C {^1H} NMR (100.6 MHz): δ 9.4 (s, PCH_2CH_3), 17.6 (d, $^1J_{PC}$ = 16 Hz, PCH_2CH_3), 38.9 (s, CCH_3), 45.0 (s, CCH_3). ^{31}P {^1H} NMR (162.0 MHz): δ −13.6 (s).

*$[Cu(PMe_3)_4][Cu_5(S^tBu)_6]$ (**3**).* To a suspension of **1** (1.004 g; 6.57 mmol) in THF (30 mL) was added PMe_3 (0.58 mL; 0.50 g; 6.57 mmol) via cannula. Compound **1** dissolved to form a yellow solution which was stirred in the dark overnight, filtered, evaporated to 5−10 mL, and slowly cooled to −40 °C. After 1 day, small amounts of brown powder were filtered off, and 3 days later large yellow blocks were collected, washed with 20 mL of Et_2O at −30 °C, and dried in vacuo at 25 °C for 2 h. Yield: 0.705 g (0.578 mmol; 53%). Anal. Calcd for $C_{36}H_{90}Cu_6P_4S_6$ (1220.67): C, 35.42; H, 7.43. Found: C, 35.33; H, 7.62. NMR (THF-d_8, [ppm]) ^1H NMR (400.6 MHz, rt): δ 1.32 (4 H, s, PCH_3), 1.45 (6 H, s, $SCCH_3$). ^{13}C {^1H} NMR (100.6 MHz): δ 17.7 (br, PCH_3), 38.6 (s, CCH_3), 44.4 (s, CCH_3). ^{31}P {^1H} NMR (162.2 MHz, rt): δ 37.6 (q, $^1J(^{63}Cu/^{31}P)$ = 788 Hz), −47.7 (br).

*$[(CuS^tBu)_6(PMe_3)_2]$ (**4**).* Compound **1** (0.609 g; 3.99 mmol) was suspended in toluene (15 mL), and PMe_3 (0.16 mL; 0.14 g; 1.8 mmol) was added via syringe. The starting material dissolved within 1−2 min to form a yellow solution which was stirred overnight in the dark, then filtered, evaporated to ∼5 mL, and slowly cooled to −40 °C. After 5 days, yellow blocks were collected by decantation, washed with 20 mL of pentane, and dried for 1 h at 25 °C. Yield: 0.265 g (0.248 mmol; 37%). Anal. Calcd for $C_{30}H_{72}Cu_6P_2S_6$ (1068.51): C, 33.72; H, 6.79; Cu, 35.68; P, 5.89; S, 18.0. Found: C, 33.80; H, 6.88; Cu, 34.9; P, 5.68; S, 17.4. NMR (toluene-d_8, rt, [ppm]) ^1H NMR (400.6 MHz): δ 1.02 (18 H, d, $^2J_{PH}$ = 6 Hz, PCH_3), 1.67 (54 H, s, $SCCH_3$). ^{31}P {^1H} NMR (162.2 MHz, rt): δ −51.2 (s).

*$[(CuS^tBu)_8(PMe_3)_2]$ (**5**).* PMe_3 (1.37 mL of 1.0 M solution in toluene) was added to a suspension of **1** (0.631 g; 4.13 mmol) in toluene (30 mL) at 25 °C. After 20 min, the yellow solution was

(11) (a) Reichle, W. T. *Inorg. Chim. Acta* **1971**, *5*, 325. (b) Dance, I. G.; Fitzpatrick, L. J.; Scudder, M. L. *J. Chem. Soc., Chem. Commun.* **1983**, 546. (c) Dance, I. G.; Guerney, P. J.; Rae, A. D.; Scudder, M. L. *Inorg. Chem.* **1983**, *22*, 2883. (d) Dance, I. G.; Scudder, M. L.; Fitzpatrick, L. J. *Inorg. Chem.* **1985**, *24*, 2547. (e) Khan, M. A.; Kumar, R.; Tuck, D. G. *Polyhedron* **1988**, *7*, 49. (f) Dance, I. G.; Fitzpatrick, L. J.; Craig, D. C.; Scudder, M. L. *Inorg. Chem.* **1989**, *28*, 1853. (g) Kumar, R.; Tuck, D. G. *Inorg. Chem.* **1990**, *29*, 1444.

(12) Schneider, S.; Roberts, J. A. S.; Salata, M. R.; Marks, T. J. *Angew. Chem., Int. Ed.* **2006**, *45*, 1733.

(13) Engel, P. S.; Pan, L.; Whitmire, K. H.; Guzman-Jimenez, I.; Willcott, M. R.; Smith, W. B. *J. Org. Chem.* **2000**, *65*, 1016.

Table 1. Crystallographic Data for the Compounds 2−5

	2a	**2b**	**3**·2THF	**4**	**5**
empirical formula	$C_{22}H_{54}Cu_4P_2S_4$	$C_{28}H_{66}Cu_4P_2S_4$	$C_{44}H_{106}Cu_6O_2P_4S_6$	$C_{30}H_{72}Cu_6P_2S_6$	$C_{52}H_{106}Cu_8P_2S_8$
formula weight	762.99	847.15	1364.88	1068.42	1558.11
crystal color	colorless	colorless	yellow	yellow	yellow
crystal size, mm	0.11 × 0.14 × 0.17	0.30 × 0.32 × 0.48	0.09 × 0.14 × 0.22	0.16 × 0.20 × 0.20	0.26 × 0.51 × 0.52
crystal system	monoclinic	monoclinic	monoclinic	monoclinic	triclinic
space group	$P2_1/n$	$P2_1/c$	$P2_1/c$	Pn	$P\bar{1}$
a, Å	10.086(2)	8.8065(6)	18.353(4)	10.7396(10)	14.509(2)
b, Å	17.585(5)	11.6863(8)	18.319(4)	10.7984(10)	14.509(2)
c, Å	10.811(3)	19.7851(14)	20.182(5)	20.278(2)	19.946(3)
β, deg	111.538(7)	96.1340(10)	94.346(4)	93.610(2)	77.194(2)
γ, deg	90	90	90	90	61.54
V, Å^3	1783.5(7)	2024.5(2)	6766(3)	2347.0(4)	3566.5(10)
Z	2	2	8	2	2
D_{calcd}, g cm^{-3}	1.421	1.390	1.269	1.512	1.451
T, K	153(2)	153(2)	153(2)	153(2)	153(2)
μ/mm^{-1}	2.686	2.374	2.156	3.024	2.646
max θ, deg	28.59	28.81	28.85	28.81	29.35
$h/k/l$ ranges	−13, 13/ −23, 23/ −14, 14	−11, 11/ −15, 15/ −26, 26	−24, 23/ 0, 24/ 0, 26	−14, 13/ −14, 14/ −27, 26	−19, 19/ −19, 19/ −26, 26
collected reflections	15423	18394	17362	20830	46017
unique reflections, n	4242	4917	17362	10762	17548
R_{int} [$I > 2\sigma(I)$]	0.0976	0.0672	0	0.0523	0.0459
parameters, p	154	181	547	422	792
refinement method	full-matrix on F^2	full-matrix on F^2	full-matrix on F^2	full-matrix on F^2	full-matrix on F^2
R_1,[a] wR_2[b] [$I > 2\sigma(I)$]	0.0397, 0.0890	0.0275, 0.0732	0.0756, 0.2053	0.0334, 0.0738	0.0287, 0.0643
R_1, wR_2 (all data)	0.0593, 0.0968	0.0302, 0.0750	0.1205, 0.2351	0.0438, 0.0777	0.0421, 0.0672
GOF[c]	1.068	1.036	1.024	0.991	0.969
largest peak/hole (e·Å^{-3})	1.028/−0.390	0.778/−0.505	1.511/−0.608	0.938/−0.384	0.588/−0.550

[a] $R_1 = \Sigma||F_0|-|F_c||/\Sigma|F_0|$. [b] $wR_2 = \{\Sigma[w(F_0^2 - F_c^2)^2]/\Sigma[w(F_0^2)^2]\}^{1/2}$. [c] GoF $= S = \{\Sigma[w(F_0^2 - F_c^2)^2]/(n-p)\}^{1/2}$.

filtered, evaporated to ∼15 mL, and stored at −40 °C. The resulting yellow crystals were subsequently collected by decantation, washed with 20 mL of pentane at −45 °C, and dried at 25 °C in vacuo for 3 h. Yield: 0.349 g (2.03 mmol; 49%). Anal. Calcd for $C_{38}H_{90}Cu_8P_2S_8$ (1373.96): C, 33.22; H, 6.60. Found: C, 33.45; H, 6.87. NMR (toluene-d_8, rt, [ppm]) ^{1}H NMR (400.6 MHz): δ 1.01 (18 H, d, $^2J_{PH}$ = 6 Hz, PCH_3), 1.68 (72 H, s, SCCH_3). ^{31}P {^{1}H} NMR (162.2 MHz, rt): δ −51.2 (s).

Crystal Structure Determinations. Single crystals of $(CuS^tBu)_4(PEt_3)_2$ (**2b**), $Cu(PMe_3)_4^+Cu_5(S^tBu)_6^-$ (**3**), $(CuS^tBu)_6(PMe_3)_2$ (**4**), and $(CuS^tBu)_8(PMe_3)_2$ (**5**) suitable for X-ray diffraction (XRD) were obtained by slow cooling of saturated diethyl ether (**2b**), diethyl ether/THF (**3**), or toluene (**4**, **5**) solutions. Crystals were transferred onto a glass slide and coated with Infineum V8512 oil, and a suitable crystal was then selected under a microscope using plane-polarized light. The crystal was mounted on a glass fiber and transferred to a Bruker SMART 1000 CCD area detector diffractometer in a N_2 cold stream at 153(2) K. Twenty frames (20 s exposures, 0.3° slices) were collected in three areas of space to determine the orientation matrix. The parameters for data collection were determined by the peak intensities and widths from the 60 frames used to determine the orientation matrix. The faces of the crystal were then indexed, and data collection was begun. After data collection, the frames were integrated, the initial crystal structure was solved by direct methods, the structure solution was expanded through successive least-squares cycles, absorption corrections were applied, and the final solution was determined. The structure of **3** was solved as a non-merohedral twin. The twin law was found with the program CELLNOW and implemented into SHELXL97 via HKLF5. Crystal, data collection, and refinement parameters are summarized in Table 1.

Results

Syntheses. Moderately air-sensitive $(CuS^tBu)_4(PEt_3)_2$ (**2b**) can be synthesized in high yield analogously to $(CuS^tBu)_4(PMe_3)_2$ (**2a**) by reaction of $(CuS^tBu)_\infty$ (**1**) with 0.5 equiv of PEt_3 in diethyl ether (Scheme 1).[9] Colorless product complexes **2a**/**b** were characterized by combustion analysis, multinuclear solution NMR, solid state ^{31}P NMR (**2a**), mass spectrometry, TGA, and single-crystal XRD. Compounds **2a**/**b** dissolve readily in toluene, Et_2O, CH_2Cl_2, and THF. However, unlike complex **2b**, **2a** forms bright yellow solutions in polar organic solvents such as CH_2Cl_2 or THF. Furthermore, prolonged stirring of **2a** in Et_2O (overnight) results in the precipitation of a yellow solid, which can be redissolved by addition of THF. Subsequent isolation of **2a** from Et_2O/THF mixtures leads to cocrystallization of substantial quantities of yellow $Cu(PMe_3)_4^+Cu_5(S^tBu)_6^-$ (**3**), which was characterized by single-crystal XRD. Ion pair **3** can be prepared in analytical purity by reaction of **1** with 1.0 equiv of PMe_3 in THF and was fully characterized. Compound **3** is soluble in THF and CH_2Cl_2 but insoluble in nonpolar solvents such as toluene. To further elucidate the structural chemistry and solution reactivity properties of the CuS^tBu/PMe_3 system, toluene suspensions of **1** were treated with PMe_3 in varying stoichiometries. Cluster complex $(CuS^t$-

Scheme 1. Syntheses of Copper(I) *tert*-Butylthiolato Trialkylphosphine Clusters 2−5

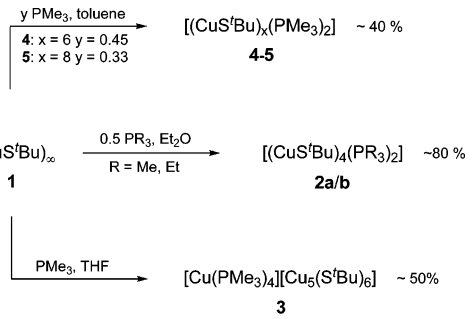

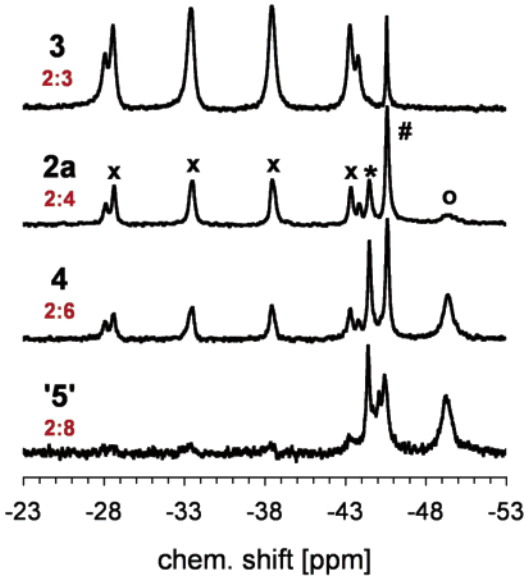

Figure 1. Solution ^{31}P NMR spectra of compounds **2a**, **3**, **4**, and the product with a P/Cu ratio of 2:8 (denoted "**5**") in THF-d_8 at −40 °C. P/Cu ratios are indicated in red.

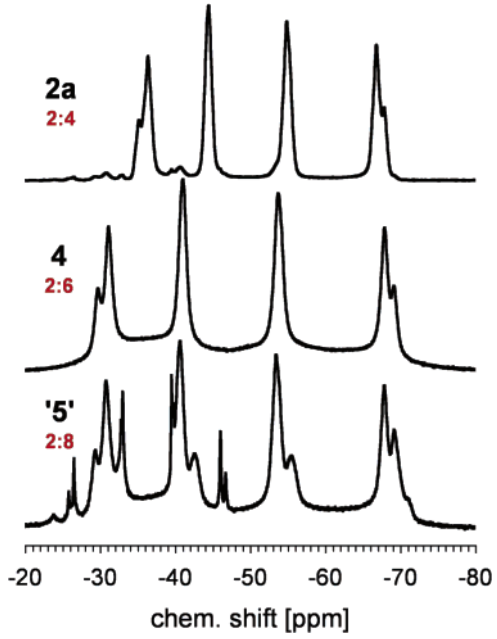

Figure 2. Solid state ^{31}P MAS NMR spectra (spinning frequency = 8 kHz) of compounds **2a**, **4** and the product with a P/Cu ratio of 2:8 (denoted "**5**"). PMe_3/Cu ratios are indicated in red.

$Bu)_6(PMe_3)_2$ (**4**) can be obtained analytically pure in moderate yields and was characterized by elemental analysis, multinuclear solution NMR, solid state ^{31}P NMR, and single-crystal XRD. Pale-yellow complex **4** is soluble in toluene and CH_2Cl_2, albeit less so than are compounds **2a**/**b**. Furthermore, the reaction of **1** with 0.33 equiv of PMe_3 yields yellow crystals with the combustion analysis indicating a CuS^{t}Bu/PMe_3 ratio of 4:1. Complex $(CuS^tBu)_8(PMe_3)_2$ (**5**) was characterized by single-crystal XRD. However, NMR analysis shows that the product consists of a mixture of cuprous thiolato phosphine clusters, both in solution and in the solid state, including considerable amounts of complex **4** (see below).

NMR Studies. The ^{1}H and ^{31}P NMR spectra of isostructural clusters **2a** and **2b** as well as compounds **4** and **5** in

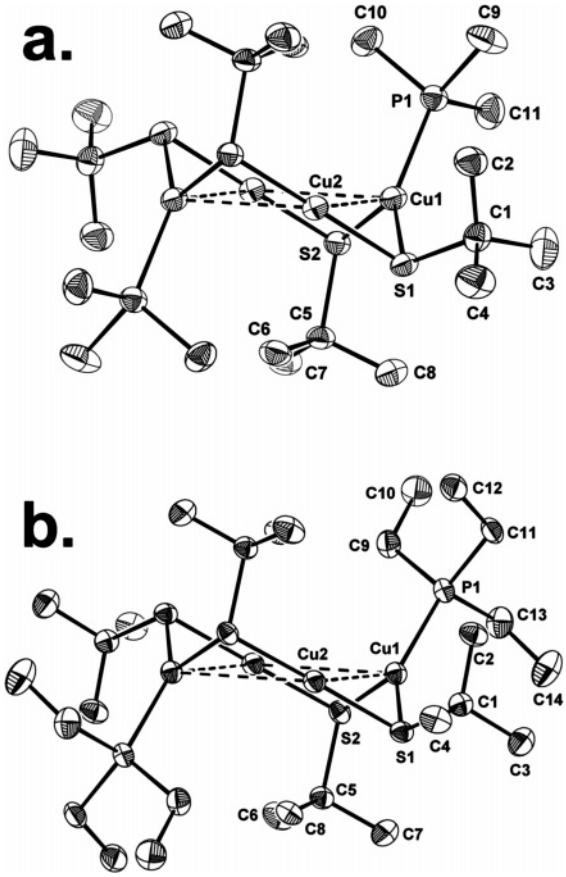

Figure 3. Solid-state molecular structures of $(CuS^tBu)_4(PR_3)_2$ complexes (**a**, R = Me (**2a**),[9] **b**, R = Et (**2b**)) with thermal ellipsoids drawn at the 50% probability level. Hydrogen atoms are omitted for clarity.

toluene-d_8 solution exhibit one set of resonances each for the thiolato and phosphine ligands, respectively. The spectra of **2a** and **2b** remain virtually unchanged upon cooling to −70 °C, while peak-broadening of the complex **4** ^{1}H signals is observed at −40 °C. In the case of **5**, three signals are observed in the ^{31}P NMR spectrum, one of them assignable to cluster **4**, suggesting phosphine ligand exchange equilibria between different cluster species, which are rapid on the NMR time scale at room temperature. In THF-d_8, PEt_3 complex **2b** exhibits a single set of resonances both at room and at low temperatures (−50 °C), strongly contrasting with trimethylphosphine complexes **2a**, **3**, and **4**. THF-d_8 and CD_2Cl_2 solutions of **2a** at room temperature exhibit additional broad features between δ −25 and δ −45 ppm in the ^{31}P NMR spectrum and generally broadened peaks in the ^{1}H and ^{31}P NMR. Cooling of these solutions below −20 °C reveals decoalescence of the thiolate and PMe_3 signals in the ^{1}H and ^{31}P spectra into multiple resonances, confirming ligand exchange equilibria at room temperature which are fast on the NMR time scale in these solvents. The ^{31}P NMR spectrum of **2a** at −40 °C in THF-d_8 features two sharp singlets at δ −45.6 (#, Figure 1) and −44.6 ppm (*), respectively, a broad signal at δ −49.6 ppm (○), and a doublet of quartets centered at δ −36.1 ppm (×). The multiplicity of the latter indicates P−Cu coupling with a ratio of $^1J_{Cu,P}$ coupling constants (1.066) in good agreement with the ratio of the copper isotope gyromagnetic moments

Table 2. Selected Bond Lengths and Bond Angles in $(CuS^tBu)_4(PR_3)_2$ Complexes 2a[9] and 2b

	2a	2b		2a	2b
		Bond Lengths (Å)			
Cu1−Cu2	2.8733(7)	2.8092(3)	Cu1−Cu2A	2.9483(9)	3.286(1)
Cu1−S1	2.2331(9)	2.2313(4)	Cu1−S2	2.2970(9)	2.2894(4)
Cu2−S2	2.1603(9)	2.1533(5)	Cu2−S1A	2.1629(9)	2.1611(4)
Cu1−P1	2.2381(9)	2.2423(5)			
		Bond Angles (deg)			
Cu2−Cu1−Cu2A	77.55(2)	75.65(2)	Cu1−Cu2−Cu1A	102.45(2)	104.35(2)
S1−Cu1−P1	138.25(3)	139.62(2)	S2−Cu1−P1	103.07(4)	100.79(2)
S1−Cu1−S2	118.09(3)	118.30(2)	S1A−Cu2−S2	173.57(4)	176.47(2)
Cu1−S1−Cu2	84.23(4)	79.50(2)	Cu1−S2−Cu2A	80.21(3)	95.36(2)

($\gamma(^{65}Cu)/\gamma(^{63}Cu) = 1.071$).[14] The large nuclear quadrupole moments of the copper nuclei (both $I = 3/2$) and well-resolved quartets suggest in this case a highly symmetrical essentially cubic coordination environment about the metal ion.[15] Therefore, this signal is assigned to the $[Cu(PMe_3)_4]^+$ cation, with both chemical shift and $^1J_{Cu,P}$ coupling constants being in excellent agreement with literature values and the ^{31}P NMR spectrum of $Cu(PMe_3)_4^+Cu_5(S^tBu)_6^-$ (**3**) in THF-d_8 at −40 °C (Figure 1).[16] The ^{31}P NMR spectra of compound **4** in THF-d_8 reveal the same type of equilibria upon cooling (Figure 1). The differing resonance integrals compared with the spectra of **2a** and **3** are in accord with the lower CuS^t-Bu/PMe_3 ratio in **4**. Likewise, the product with the Cu/P ratio of 4:1 ("**5**") consists of an equilibrium mixture of different thiolate phosphine species, with the ^{31}P NMR in THF-d_8 at −40 °C exhibiting the same trend in relative peak ratios as for compounds **2a**, **3**, and **4** (Figure 1).

The solid state ^{31}P NMR spectrum of compound **2a** (Figure 2) exhibits one set of resonances for the two PMe_3 ligands. Equivalent chemical shift tensors for the two phosphorus atoms are in agreement with the solid-state structure derived by XRD featuring an equivalence of phosphine ligands via a crystallographic inversion center (Figure 3a).[17] Coupling with spin 3/2 ^{63}Cu results in a quartet multiplicity, and even ^{65}Cu satellites are resolved for the outermost peaks. The quartet is distorted with inequivalent line separations as a result of scalar J coupling combined with dipolar and anisotropic J coupling.[18] The $^1J(^{63}Cu,^{31}P)$ coupling constant (1270 Hz) is represented by the central line spacing ($\Delta\nu_2$) within the quartet. The scalar J coupling constant and the Cu−P bond length d are in agreement with an empirically found linear relationship between $1/d^3$ and J for a series of copper triarylphosphine complexes, confirming trigonal planar coordination geometry.[19] The ratio of the quartet line spacings at higher and lower field ($\Delta\nu_3/\Delta\nu_1 = 1.48$), which correlates to a first approximation with the asymmetry of the electric field gradient tensor around the quadrupolar nucleus, is in the range typically observed for three-coordinate copper.[17] The ^{31}P MAS NMR spectrum of **4**, which features PMe_3 bound to three-coordinate copper centers as well, strongly resembles that of **2a** with one signal exhibiting very close chemical shift and quartet multiplicity with similar Cu−P coupling characteristics ($\Delta\nu_2 = 1542$ Hz/d_{av}(Cu−P) = 2.205 Å; $\Delta\nu_3/\Delta\nu_1 = 1.43$). However, according to the crystal structure the two phosphorus atoms should be chemically inequivalent. It thus remains unclear whether the two phosphorus nuclei accidentally exhibit very similar chemical shifts, which are not resolved in the spectrum. Finally, the ^{31}P MAS NMR spectrum of the product with a P/Cu ratio of 2:8 (Figure 2, "**5**") features a mixture of clusters. The principal quartet is identical with that of cluster **4**. A further very sharp quartet is assigned to the $Cu(PMe_3)_4^+$ cation because the multiplet interline distances ($\Delta\nu_3/\Delta\nu_1 = 1.00$) indicate high symmetry around Cu, and the chemical shift (δ 36.3 ppm) and the Cu−P coupling constant (790 Hz) are in excellent agreement with solution ^{31}P NMR data for ion pair **3**. Other compounds are indicated by weaker signals at δ −23.8, −42.7, −55.5, and −71.0 ppm. However, overlap with the more prominent resonances renders assignments, for example, to cluster **5**, impossible.

Crystal Structure Analyses. The isostructural, tetranuclear clusters **2a**[9] and **2b** are C_i symmetric with the crystallographic inversion center at the center of the planar, rectangular arrangement of the Cu_4 parallelogram (Figure 3 and Table 2). Each pyramidalized sulfur atom bridges two adjacent copper centers resulting in nearly ideally linear (Cu2, Cu2A) and trigonally planar (Cu1, Cu1A) coordination geometries, respectively. The only other structurally characterized tetrameric mixed thiolato phosphine copper complex, $(CuS^tBu)_4(PPh_3)_2$, exhibits the same "chairlike" coordination geometry of the eight-membered Cu_4S_4 ring.[11c] The phosphine ligands complete the coordination spheres of Cu1 and Cu1A at opposite sides of the central Cu_4 plane, located above and below the cluster, respectively. The Cu−Cu distances within the Cu4 plane define the major difference between the two structures, with a shorter Cu1−Cu2 distance and considerably longer Cu1−Cu2A distance in **2b**. The Cu−S−Cu bond angles are accordingly adjusted, consistent with the marked conformational flexibility in low-coordinate copper(I) thiolato complexes.[20] Clusters **2**−**5** all contain copper in the +1 oxidation state, so that formal Cu−Cu bonding between the d^{10} centers can be neglected except via weak correlation effects.[21]

Ion pair $Cu(PMe_3)_4^+Cu_5(S^tBu)_6^-$ (Figure 4, Table 3) exhibits no contact distances between anion and cation in

(14) Wu, G.; Wasylishen, R. E. *Inorg. Chem.* **1996**, *35*, 3113.
(15) Verkade, J. G.; Mosbo, J. A. In *Phosphorous-31 NMR Spectroscopy in Stereochemical Analysis*; Verkade, J. G., Quinn, L. D., Eds.; VCH: Deerfield Beach, 1987.
(16) (a) Dempsey, D. F.; Girolami, G. S. *Organometallics* **1988**, *7*, 1208. (b) Chi, K.-M.; Farkas, J.; Hampden-Smith, M. J.; Kodas, T. T.; Duesler, E. N. *J. Chem. Soc., Dalton Trans.* **1992**, 3111.
(17) Nelson, J. H. *Concepts Magn. Reson.* **2002**, *14*, 19.
(18) (a) Olivieri, A. *J. Am. Chem. Soc.* **1992**, *114*, 5758. (b) Bowmaker, G. A.; Hanna, J. V.; Hart, R. D.; Healy, P. C.; White, A. H. *J. Chem. Soc., Dalton Trans.* **1994**, 2621.
(19) Menger, E. M.; Veemann, W. S. *J. Magn. Reson.* **1982**, *46*, 257.
(20) Henkel, G.; Krebs, B. *Chem. Rev.* **2004**, *104*, 801.
(21) Pyykkö, P. *Chem. Rev.* **1997**, *97*, 597.

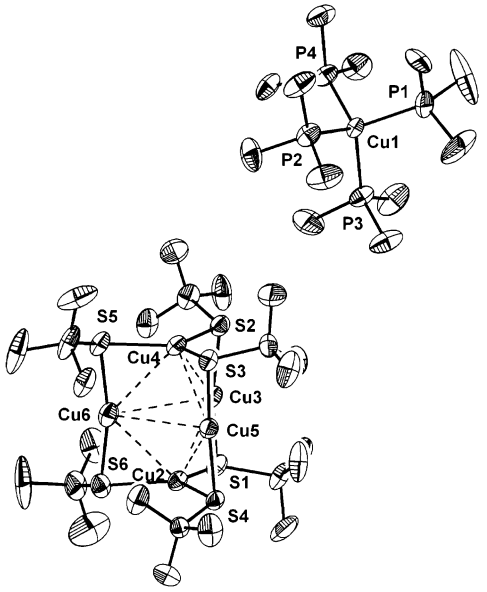

Figure 4. Molecular structure of $Cu(PMe_3)_4^+Cu_5(S^tBu)_6^-$ (**3**) in the crystal with thermal ellipsoids drawn at the 40% probability level. Hydrogen atoms, THF solvent molecules, and split positions for C1−C3 in $Cu(PMe_3)_4^+$ cluster cation are omitted for clarity.

the molecular structure that are significantly shorter than the sum of the respective van der Waals radii.[22] In the cation, the almost ideally tetrahedrally coordinated copper center (Cu1) exhibits mean Cu1−P bond lengths and P−Cu1−P angles which are identical to those reported in the literature.[16] The copper atoms of the $Cu_5(S^tBu)_6^-$ cluster anion core, Cu2−Cu6, form a Cu_5 trigonal bipyramid. All edges of the polyhedron not lying in the trigonal plane are capped by S^t-Bu ligands. Consequently, the six sulfur atoms describe a trigonal prismatic S_6 cage. The two parallel triangular faces of the prism, defined by S1/S4/S6 and S2/S3/S5, respectively, are almost perfectly eclipsed as indicated by their mean dihedral angle with the edges of the prism described by straight lines through S1/S2, S3/S4, and S5/S6, respectively ($\theta = 87.4°$), which is close to the ideal value (90°). In contrast, the two triangular faces that define the S_6 polyhedron in $NEt_3R^+Cu_5(S^tBu)_6^-$ (R = H, Et)[24] exhibit considerably larger antiprismatic twists (mean $\theta = 64.4°$, 62.3°), respectively, compared with **3**. The only other structurally characterized derivative, the $Cu_5(SAd)_6^-$ anion bearing bulky 1-adamantylthiolato ligands, exhibits an even larger twist (mean $\theta = 55.2°$).[23] The low coordination number of the copper atoms accounts for the low energetic barriers of S_6 cage distortion, the high thermal motion of the metal centers in the solid state, and the structural non-rigidity in solution. Henkel and Krebs pointed out that the $Cu_5(SR)_6^-$ anion is therefore the preferred species for thiolates with sterically demanding substituents R.[20] The superposition of the Cu_5 and S_6 polyhedra in the cluster anion of **3** results in trigonal-planar coordination for Cu2 and Cu4. Hence, they exhibit considerably longer Cu−S distances than linear two-coordinate Cu3, Cu5, and Cu6. The orientation of the *tert*-butyl substituents finally results in idealized D_3 symmetry for the entire cluster anion.

The molecular structure of **4** (Figure 5, Table 4) can best be described starting from the $Cu_5(S^tBu)_6^-$ cluster anion in ion pair **3** (Figure 6). Atoms Cu1−Cu4 define a trigonal pyramid, which is edge-capped by thiolate ligands S3, S4, and S6, resembling one-half of the trigonal bipyramidal Cu_5 cluster core in $Cu_5(S^tBu)_6^-$ (see above), with almost identical geometrical parameters around trigonal planar Cu1 and only small deviations for linearly coordinated Cu2−Cu4. However, the second apex of the Cu_5 bipyramid in **3** has been removed in **4** by coordination of PMe_3 to Cu6 and concomitant cleavage of a Cu−S bond, fragmenting the closed $Cu_5(S^tBu)_6^-$ structure to form more open $Cu_5(S^tBu)_6PMe_3^-$. Charge balance in **4** is achieved by coordination of an additional $CuPMe_3^+$ fragment to S1 and S2 at the periphery of the $Cu_5(S^tBu)_6^-$ framework, rendering **4** the formal product of electrophilic attack of a $Cu(PMe_3)_2^+$ cation on the cluster anion of ion pair **3**.

Central to the structure of octameric thiolato cluster **5** (Figure 7, Table 5) is a planar, rectangular arrangement of Cu1, Cu3, Cu5, and Cu7, with edges bridged by thiolato ligands S1, S2, S4, and S5. The resulting eight-membered ring is reminiscent of tetranuclear **2a** and **2b** as shown in Figure 8. Two opposite copper atoms are distorted linearly coordinated (Cu1, Cu7). The other two copper atoms (Cu3, Cu5) exhibit trigonal planar coordination to additional thiolates (S3, S6), instead of bearing phosphine ligands as in **2**. Thiolato ligands S1 and S2 and CuS^tBu fragments Cu4−S3 and Cu2−S6 bridge the $(CuS^tBu)_4$ moiety with a $\{CuS^tBu(PMe_3)\}_2$ unit which itself exhibits a planar Cu_2S_2 square with four-coordinate copper (Cu6, Cu8) and sulfur (S7, S8) atoms, respectively. This arrangement results in a pseudo-C_2 axis through Cu1, Cu7, and the center of the Cu_2S_2 square, consistent with the equivalency of the two PMe_3 ligands in the solution ^{31}P NMR. Cu−S bond lengths for two-coordinate (Cu1, Cu2, Cu4, Cu7), three-coordinate (Cu3, Cu5), and four-coordinate (Cu6, Cu8) are in the typical range for copper(I) thiolato complexes.[11]

Precursor Thermal Stabilities. Complexes **2**−**5** are stable in solution (toluene, CH_2Cl_2, THF) at room temperature by ^1H and ^{31}P NMR over the course of several weeks if stored in the dark. However, exposure to ambient light leads to decomposition accompanied by visible darkening after several hours. The compositional and thermal stabilities of precursors **2a**,**b** were further examined by chemical ionization (CI-MS) and electrospray mass spectrometry (ESI-MS). The CI-MS of compound **2b** resembles that of $(CuS^tBu)_\infty$ (**1**); that is, the tetrameric cluster cation $(CuS^tBu)_4^+$ ($m/z = 610.6$) is both the strongest (55%) and heaviest copper gas-phase species observed between $0 < m/z < 900$, with all other copper-containing peaks ranging in intensity below 5%, consistent with the complete loss of the phosphine ligands prior to sublimation. ESI-MS of **2a** and **2b** in CH_2Cl_2 between $0 < m/z < 2000$ (Figure 9) reveals a distribution of oligomeric cluster cations having the general formula $Cu_{x+1}(S^tBu)_x(PR_3)_y^+$ (R = Me (**2a**), Et (**2b**)). Typically, within one run, the ion distribution broadens toward higher

(22) Bondi, A. *J. Phys. Chem.* **1964**, *68*, 441.
(23) Fujisawa, K.; Imai, S.; Kityjima, N.; Moro-oka, Y. *Inorg. Chem.* **1998**, *37*, 168.
(24) (a) Dance, I. G. *J. Chem. Soc., Chem. Commun.* **1976**, 68. (b) Bowmaker, G. A.; Clark, G. R.; Seadon, J. K.; Dance, I. G. *Polyhedron* **1984**, *3*, 535.

Table 3. Selected Bond Lengths and Bond Angles of Compound 3·2THF

Bond Lengths (Å)							
Cu1−P1	2.262(3)	Cu1−P2	2.269(3)	Cu1−P3	2.259(2)	Cu1−P4	2.260(2)
Cu2−S1	2.248(2)	Cu2−S4	2.244(2)	Cu2−S6	2.259(2)	Cu3−S1	2.166(2)
Cu3−S2	2.153(3)	Cu4−S2	2.250(2)	Cu4−S3	2.251(2)	Cu4−S5	2.250(2)
Cu5−S3	2.162(2)	Cu5−S4	2.158(2)	Cu6−S5	2.150(3)	Cu6−S6	2.158(3)

Bond Angles (deg)					
P1−Cu1−P2	108.16(13)	P1−Cu1−P3	110.08(11)	P1−Cu1−P4	109.72(12)
P2−Cu1−P3	108.59(10)	P2−Cu1−P4	109.57(10)	P3−Cu1−P4	110.67(9)
S1−Cu2−S4	119.70(8)	S1−Cu2−S6	119.75(9)	S4−Cu2−S6	120.02(9)
S1−Cu3−S2	166.66(10)	S2−Cu4−S3	120.74(9)	S2−Cu4−S5	119.15(9)
S3−Cu4−S5	119.82(9)	S3−Cu5−S4	167.56(9)	S5−Cu6−S6	167.30(10)

Table 4. Selected Bond Lengths and Bond Angles of Compound 4

Bond Lengths (Å)					
Cu1−S3	2.2632(11)	Cu1−S4	2.2547(11)	Cu1−S6	2.2474(11)
Cu2−S1	2.1755(11)	Cu2−S3	2.1743(11)	Cu3−S4	2.1853(12)
Cu3−S5	2.1732(11)	Cu4−S2	2.1786(11)	Cu4−S6	2.1702(11)
Cu5−S1	2.2999(10)	Cu5−S2	2.2644(10)	Cu5−P2	2.2086(12)
Cu6−S1	2.3446(11)	Cu6−S5	2.2314(11)	Cu6−P1	2.2009(12)

Bond Angles (deg)					
S3−Cu1−S4	121.47(4)	S3−Cu1−S6	119.27(4)	S4−Cu1−S6	119.25(4)
S1−Cu2−S3	162.89(4)	S4−Cu3−S5	161.10(5)	S2−Cu4−S6	168.11(4)
S1−Cu5−S2	92.47(4)	S1−Cu5−P2	128.84(4)	S2−Cu5−P2	138.36(5)
S1−Cu6−S5	102.15(4)	S1−Cu6−P1	120.42(4)	S5−Cu6−P1	137.03(5)

retention times, tentatively explained by fast thiolato cluster size equilibration upon volatile phosphine loss. In the case of **2a** (Figure 9a,b), the most abundant cations lie in the range $Cu_{x+1}(S^tBu)_x(PMe_3)_y^+$ where $x = 6 \pm 1$ and $y = 2 \pm 1$. Because of the nearly identical masses of the CuS^tBu fragment (152.0 *m*/*z*) and two PMe_3 ligands (152.1 *m*/*z*), two cluster cations within either of the series $Cu_{x-y+1}(S^tBu)_{x-y}(PMe_3)_{2y}$ or $Cu_{x-y+1}(S^tBu)_{x-y}(PMe_3)_{2y+1}$ cannot be readily distinguished. However, the isotopic patterns suggest superimposition of ions in the spectrum. For **2b** (Figure 9c) most peaks can be assigned to cluster ions with the formula $Cu_{x+1}(S^tBu)_x(PEt_3)_2^+$ ($0 \le x \le 6$) with the median of the distribution at $x = 2$. Additional cluster cations can be assigned to $Cu_8(S^tBu)_7(PEt_3)^+$ ($I = 19\%$) and $Cu_9(S^tBu)_8(PEt_3)_6^+$ ($I = 12\%$). In the negative ion mode, the ESI-MS of **2b** is dominated by the $Cu_5(S^tBu)_6^-$ cluster anion base peak, which was structurally characterized in the ion pair $Cu(PMe_3)_4^+Cu_5(S^tBu)_6^-$ (**3**). Smaller peaks with $I < 20\%$ can be assigned to $Cu(S^tBu)_2^-$ and $Cu_2(S^tBu)_3^-$. While anions of the type $Cu(SR)_2^-$ and $Cu_5(SR)_6^-$ have been structurally characterized, $Cu_2(S^tBu)_3^-$ has not been observed in the solid state. [24] Most importantly, no peaks assignable to sulfide clusters can be detected, in accord with the thermal stability of the C−S linkage under these conditions, which renders compounds **2a**,**b** ideal molecular precursors for Cu_2S deposition processes using aerosol delivery.

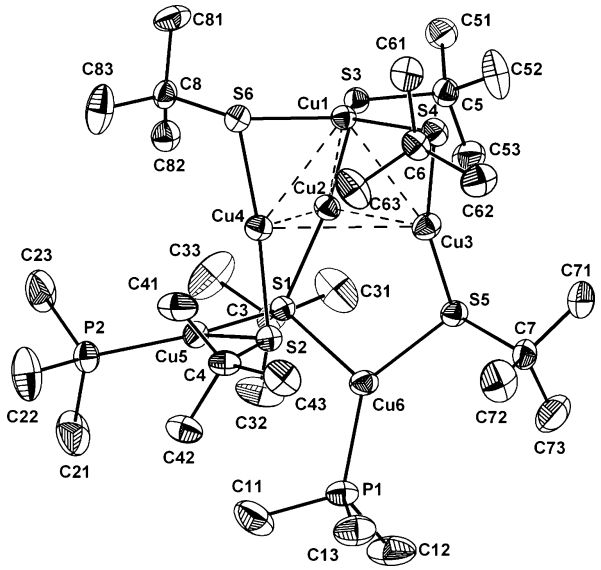

Figure 5. Molecular structure of $(CuS^tBu)_6(PMe_3)_2$ (**4**) in the crystal with thermal ellipsoids drawn at the 50% probability level. Hydrogen atoms are omitted for clarity.

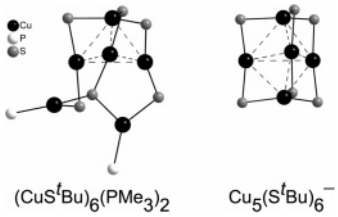

Figure 6. Comparison of the structurally related cluster cores of $(CuS^tBu)_6(PMe_3)_2$ (**4**, left) and $Cu(PMe_3)_4^+Cu_5(S^tBu)_6^-$ (**3**, right) in the crystal. *tert*-Butyl and methyl groups are omitted for clarity.

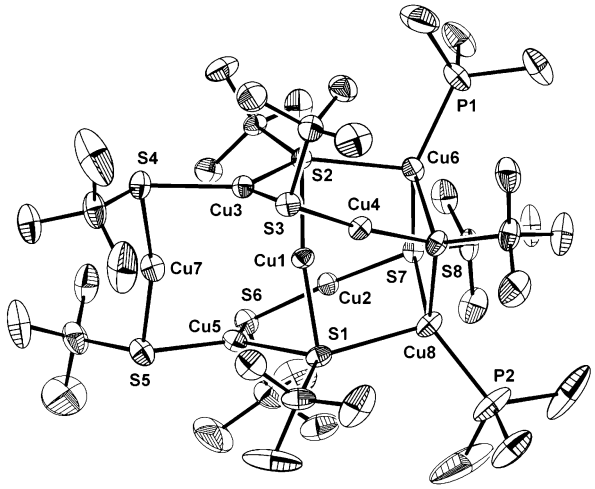

Figure 7. Molecular structure of $(CuS^tBu)_8(PMe_3)_2$ (**5**) in the crystal with thermal ellipsoids drawn at the 50% probability level. Hydrogen atoms are omitted for clarity.

Table 5. Selected Bond Lengths and Bond Angles of Compound 5

Bond Lengths (Å)							
Cu1−S1	2.1822(6)	Cu1−S2	2.1849(6)	Cu2−S6	2.1578(6)	Cu2−S7	2.1596(6)
Cu3−S2	2.3022(6)	Cu3−S3	2.3034(6)	Cu3−S4	2.2489(6)	Cu4−S3	2.1432(6)
Cu4−S8	2.1464(6)	Cu5−S1	2.3095(6)	Cu5−S5	2.2429(6)	Cu5−S6	2.3048(6)
Cu6−S2	2.4849(6)	Cu6−S7	2.4250(6)	Cu6−S8	2.3762(7)	Cu6−P1	2.2409(7)
Cu7−S4	2.1524(6)	Cu7−S5	2.1579(7)	Cu8−S1	2.4981(6)	Cu8−S7	2.3784(7)
Cu8−S8	2.3995(6)	Cu8−P2	2.2202(7)				

Bond Angles (deg)					
S1−Cu1-S2	171.19(2)	S6−Cu2−S7	176.01(2)	S2−Cu3−S3	120.78(2)
S3−Cu3−S4	122.05(2)	S2−Cu3−S4	116.73(2)	S3−Cu4−S8	174.39(2)
S1−Cu5−S5	116.29(2)	S5−Cu5−S6	122.07(2)	S1−Cu5−S6	121.48(2)
S2−Cu6−S7	101.90(2)	S2−Cu6−S8	97.918(18)	S7−Cu6−S8	88.773(18)
P1−Cu6−S2	110.34(2)	P1−Cu6−S7	126.53(2)	P1−Cu6−S8	125.80(2)
S4−Cu7−S5	166.37(2)	S1−Cu8−S7	95.662(18)	S1−Cu8−S8	103.03(2)
S7−Cu8−S8	89.325(19)	P2−Cu8−S1	112.06(3)	P2−Cu8−S7	125.28(3)
P2−Cu8−S8	125.59(3)				

The solid state thermal stabilities of compounds **1**, **2a**, **2b**, and **3** were examined by TGA and differential thermal analysis (DTA) at atmospheric pressure under an inert gas (N_2) flow of 100 mL min^{-1} (Figure 10). The endothermic peak at ∼141 °C in the DTA of **1** is accompanied by a slight color change toward orange-yellow, probably associated with a phase transition without apparent thermolysis. Endothermic thermolysis of **1** to yield α-Cu_2S is indicated by the mass loss in the TGA trace (residue: exptl, 52.0%; calcd, 52.1%) and confirmed by XRD of the residue for all four compounds and is accompanied by a broad DTA response following a sharp melting feature at 185 °C. Trialkylphosphine complexes **2a** and **2b** exhibit virtually identical TGA traces with stepwise decomposition between ∼100 °C and ∼240 °C, leaving a residue at 40.1 (**2a**) and 36.4% (**2b**), respectively, in good agreement with decomposition to Cu_2S (calcd, **2a**, 41.7%; **2b**, 37.6%).[9] The phosphine ligands dissociate over a broad temperature range, starting at ∼100 °C, close to the melting points, which are marked by sharp endothermic peaks in the DTA curves at 118 (**2a**) and 106 °C (**2b**), respectively. The shallow TGA traces in the region of PR_3 loss (Figure 10, ① and ②) are overlapped with a steeper region of mass loss (Figure 10, ③), assignable to thiolate decomposition at temperatures close to those of parent compound **1**. However, thermolysis of complexes **2a** and **2b** is complete at ∼15 °C higher temperatures than that of **1**. The two additional endothermic features in the DTA traces of **2a** at T = 137 and 148 °C are tentatively assigned to the melting points of other cluster species present, because **2a** yields a homogeneous, yellow liquid at ∼145 °C. The rich structural chemistry of compound **2a** in solution is well documented by ESI-MS and ^{31}P NMR data (see above), contrasting with the configurational stability of **2b** in the NMR. Similarly, decomposition of ion pair **3** begins with pronounced PMe_3 loss at temperatures T > 70 °C, proceeding slowly with shallow TGA and DTA curves up to ∼180 °C (Figure 10). Two broader peaks at 134 and 145 °C, similar to those in the DTA trace of **2a**, mark the melting region of **3**, suggesting the presence of multiple phosphine thiolato cluster species in the melt. The C−S bond cleavage region in the TGA and DTA at T > 180 °C resembles that of compound **1**, leaving a residue (39.8%) which is very close to the theoretical value (39.1%) for Cu_2S.

Qualitative analysis of the volatile thermolysis products of complexes **1**, **2a**, **2b**, and **3**, trapped in an offline experiment at atmospheric pressure under a stream of N_2, was carried out by ^1H and ^{31}P NMR and by GC-MS. For all four compounds, HS^tBu and isobutene are the principal volatile thiolate thermolysis products (eq 1). Furthermore, small amounts of isobutane and S^tBu_2 along with traces of $S_2{}^tBu_2$ and H_2S could also be detected. Besides these organic products, the alkylphosphines PR_3 (R = Me, **2a**, **3**; Et, **2b**) are detected for compounds **2a**/**b** and **3**, and no $R_3P{=}S$ (R = Me, Et) is present by ^{31}P NMR spectroscopy.

$$\underset{\mathbf{2}}{(CuS^tBu)_4(PR_3)_2} \xrightarrow[R=Me,Et]{\Delta T} 2Cu_2S + 2PR_3 + 2HS^tBu + 2H_2C{=}CMe_2 \quad (1)$$

Discussion

In the present study, the new trialkylphosphine stabilized *single-source* precursors **2a** and **2b** were synthesized in high

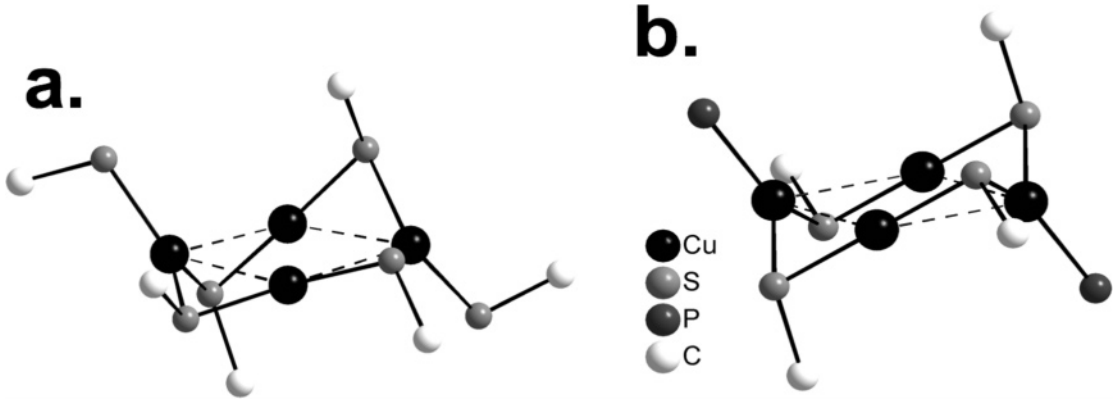

Figure 8. $(CuS^tBu)_4$ cluster core fragments of compounds **5** (a) and **2a** (b). Methyl groups omitted for clarity.

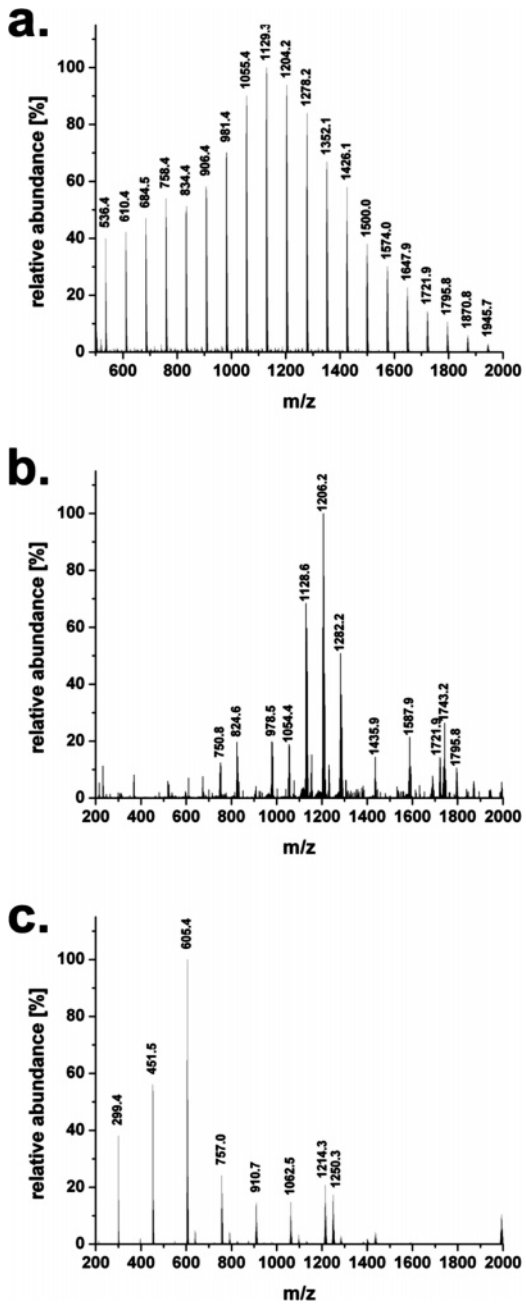

Figure 9. ESI mass spectra (positive mode) of compounds **2a** (a, b) and **2b** (c) in CH_2Cl_2.

yield. Structural characterization in solution (NMR), in the gas phase (ESI-MS), and in the solid state (^{31}P MAS NMR spectroscopy, XRD) amply documents their configurational flexibility. NMR spectra of **2a** and **2b** in toluene-d_8 are in agreement with a time-averaged pseudo-C_{2h}-symmetric structure in solution, compared with **2a**/**b** C_i symmetry in the crystal (see below), therefore suggesting a low inversion barrier for the μ_2-bridging thiolato ligands. Likewise, the ^{31}P spectrum of **4** in toluene-d_8 exhibits a single resonance at low temperatures, although two signals would be expected from the molecular structure in the solid state. Rapid equilibration between the two phosphine ligand sites on the NMR time scale in solution under the experimental conditions can be explained by racemization of the C_1 symmetric structure with small conformational change around S1, S2, and S5, and inversion of the *tert*-butyl substituent orientations

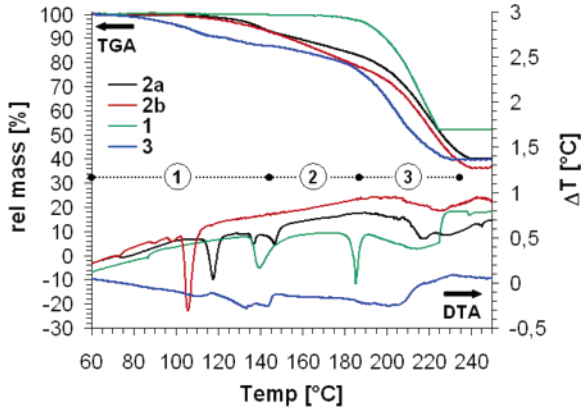

Figure 10. TGA and DTA traces of compound **1** (green), **2a** (black), **2b** (red), and **3** (blue) at atmospheric pressure under N_2 (flow rate, 100 sccm; temperature ramp, 1 °C/min).

of S3, S4, and S6 (Figure 5), suggesting a very low interconversion barrier. However, it remains unclear why cluster **4** exhibits only one signal in the ^{31}P MAS NMR spectrum for the crystallographically inequivalent phosphine ligands, with the suggested racemization process unlikely in the solid state at room temperature.[25] Note that coincidental chemical shift equivalence of two inequivalent phosphorus atoms in the ^{31}P MAS NMR spectra has been described in the literature.[26]

$$\underset{\mathbf{2a}}{(CuS^tBu)_4(PMe_3)_2} \underset{x<0.5}{\overset{THF,CH_2Cl_2}{\rightleftharpoons}} (CuS^tBu)(PMe_3)_x + \underset{\mathbf{3}}{[Cu(PMe_3)_4][Cu_5(S^tBu)_6]} \quad (2)$$

The constitutional stability of **2b** in both nonpolar (e.g., toluene) and polar (e.g., THF) organic solvents contrasts with trimethylphosphine derivative **2a** as shown by ^{31}P NMR. The driving force for the rapid equilibria observed upon dissolving the trimethylphosphine derivatives **2a**, **4**, and **5** in more polar organic solvents (THF, CD_2Cl_2) is suggested to be the formation of ion pair **3**, in accordance with the yellow color of **2a** in THF.[27] This assumption is supported by the findings that $Cu_5(S^tBu)_6^-$ is the most abundant anion in the negative mode MS, the assignment of ^{31}P NMR signal × (Figure 1) to the cation $Cu(PMe_3)_4^+$, and finally the cocrystallization of **3** with **2a** from Et_2O/THF. Simple stoichiometry considerations require the concurrent formation of compounds with smaller P/Cu ratios than **2a** in solution (eq 2), assignable to the other peaks in the ^{31}P NMR spectrum (Figure 1: #, *, ○).

Comparison of the low temperature ^{31}P NMR spectra in THF-d_8 of the compounds with descending P/Cu ratios (Cu^t-Bu)$(PMe_3)_x$ (**3**, $x = 0.67$; **2a**, $x = 0.5$; **4**, $x = 0.33$; "**5**", $x = 0.25$) suggests that the signals in Figure 1 can be assigned to species with P/Cu ratios in the order × > # > * > ○.

(25) The molecular structure was solved with two independent crystals from two independent batches of compound **4**. Although the two structural solutions exhibited different cell parameters, in principle the cluster conformation was identical with only small alterations in bond lengths and angles.

(26) Lindner, E.; Fawzi, R.; Mayer, H. A.; Eichele, K.; Hiller, W. *Organometallics* **1992**, *11*, 1033.

(27) Solvatochromic behavior was also reported for $(CuSPh)_4(PPh_3)_4$, albeit not further examined: ref 11d.

Scheme 2. Proposed Rearrangement Mechanism Connecting Thiolato Clusters 2a and 5[a]

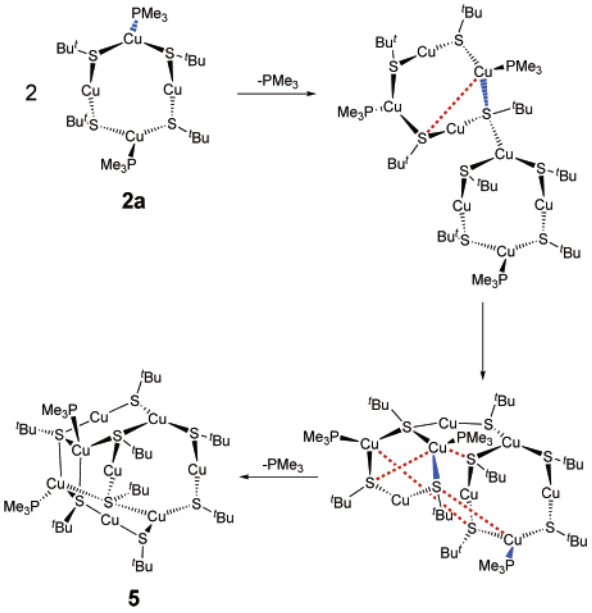

[a] Bonds to be broken are highlighted in blue, and bonds to be formed are shown with dashed red lines.

Therefore, these signals are tentatively assigned to structures **3**, **2a**, **4**, and **5**, respectively. Facile interconversion in solution of cluster compounds **2a**, **3**, **4**, and **5** is further suggested by comparison of the structures in the solid state. The feature central to all structures is a puckered Cu−S−Cu−S−Cu−S−Cu−S eight-membered ring. On the basis of their structural relationship, Scheme 2 shows a possible rearrangement pathway with the condensation of two **2a** clusters forming **5** upon release of two PMe_3 ligands. In addition to phosphine dissociation, only two Cu−S bonds must be broken for the proposed rearrangement, suggesting that this process could be very facile.

The core of the $Cu_5(S^tBu)_6^-$ cluster anion in ion pair **3** can also be described as three face-sharing Cu_4S_4 eight-membered rings which adopt, unlike the chair conformation in **2a**, roof-like conformations with pseudo-C_{2v} local symmetry to form a cylindrical object with a star-shaped cross section. Scheme 3 suggests a plausible pathway for reassembling three **2a** tetramers to form one equivalent of ion pair **3** and cluster **4**, respectively. The structure of **4** can easily be derived by the formal addition of a $Cu(PMe_3)_2^+$ fragment to $Cu_5(S^tBu)_6^-$, indicating that **4** is the primary product of **3** upon loss of PMe_3. Only five Cu−S bonds must be broken in the proposed rearrangement of the three **2a** clusters, suggesting this process to be facile.

The solution behavior of the present PMe_3 clusters contrasts with PEt_3 derivative **2b**, which is colorless and configurationally stable by ^{31}P NMR in THF and CH_2Cl_2. Similarly, Hampden-Smith and co-workers reported that, unlike ion pair $Cu(PMe_3)_4^+CuCl_2^-$, the triethylphosphine derivative is isolated as uncharged $CuCl(PEt_3)_2$.[16b] In fact, the $Cu(PEt_3)_4^+$ cation has not been reported in solution or in the solid state, presumably due to the increased steric bulk caused by the larger phosphine cone angle of PEt_3 (132°)

Scheme 3. Proposed Rearrangement of Thiolato Cluster 2a to Clusters 3 and 4[a]

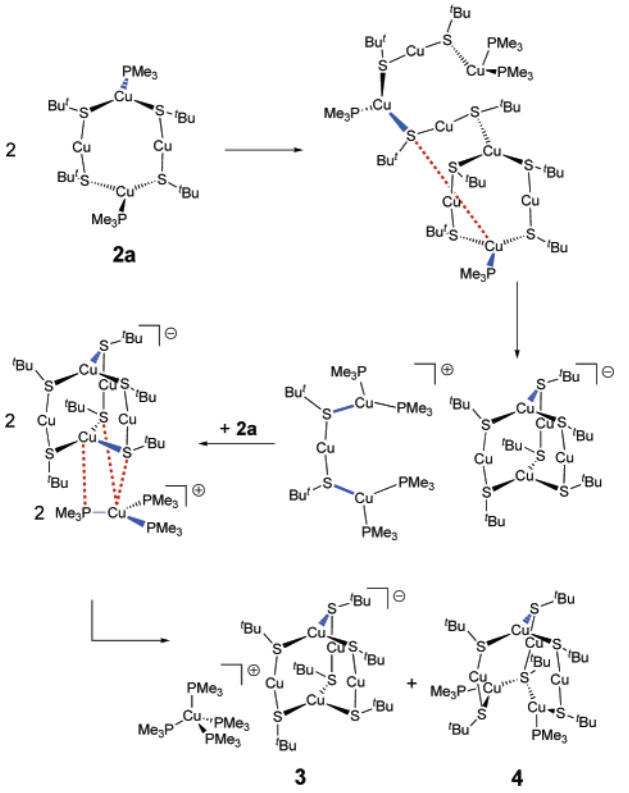

[a] Bonds to be broken are highlighted in blue, and bonds to be formed are shown with dashed red lines.

compared with that of PMe_3 (118°).[28] $Cu(PAr_3)_3^+$ species (Ar = Ph, *p*-C_6H_4OMe) are the only structurally characterized copper(I) trisphosphine cations with nonchelating phosphines and have only been observed with complex, weakly coordinating anions (PF_6^-, ClO_4^-, $V(CO)_6^-$, $FeCl_4^-$, $HCr_2(CO)_{10}^-$, and $CpMo(SC_6F_5)_4^-$).[29] Apart from steric arguments, the lability of the $Cu(PR_3)_4^+$ cation can generally be attributed to the intrinsic weakness of the copper−phosphine bonds in high coordination number complexes. Thus, Schwerdtfeger et al. showed by density functional theory calculations for the series $Cu(PH_3)_n^+$ that the dissociation energy of a single phosphine ligand is much greater for $n = 1$ (227.6 kJ/mol) and $n = 2$ (210.1 kJ/mol) than for trigonal planar ($n = 3$, 106.5 kJ/mol) or tetrahedral ($n = 4$, 96.6 kJ/mol) derivatives.[30] This general preference of the coinage metals for linear coordination is expected to also apply for the more basic trialkylphosphines, explaining the pronounced lability.

Thermal analysis of the present precursors by TGA/DTA was supplemented by offline batch thermolysis experiments to identify the volatile products because precursor concentrations during AACVD runs were too low to give definitive

(28) Tolman, C. A. *Chem. Rev.* **1977**, *77*, 313.
(29) (a) Doyle, G.; Eriksen, K. A.; Van Engen, D. *Organometallics* **1985**, *4*, 2201. (b) Baiada, A; Jardine, F. H.; Willet, R. D.; Emerson, K *Inorg. Chem.* **1991**, *30*, 1365. (c) Klüfers, P.; Wilhelm, U. *J. Organomet. Chem.* **1991**, *421*, 39. (d) Saturnino, D. J.; Arif, A. M. *Inorg. Chem.* **1993**, *32*, 4157. (e) Davidson, J. L.; Lindsell, W. E.; McCullough, K. J.; McIntosh, C. H. *Organometallics* **1995**, *14*, 3497. (f) Healy, P. C.; Hanna, J. V. *Acta Crystallogr., Sect. E* **2003**, *59*, m384.
(30) Schwerdtfeger, P.; Hermann, H. L.; Schmidbaur, H. *Inorg. Chem.*, **2003**, *42*, 1334.

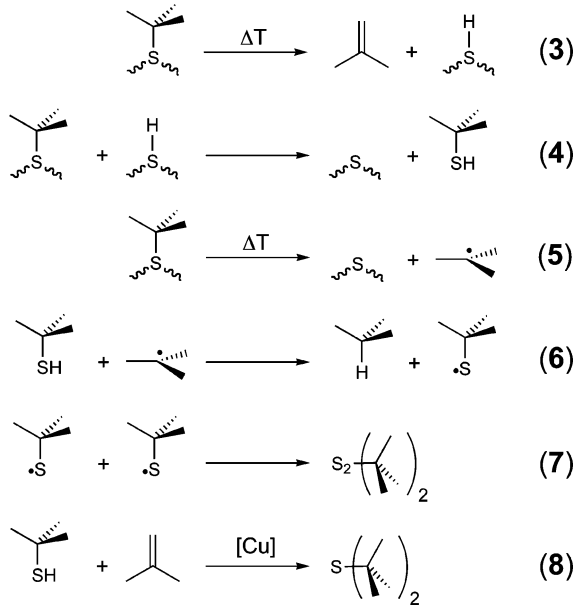

results by NMR and GC-MS.[31] We believe that these conditions should reasonably simulate the aerosol particle thermolysis pathways and provide qualitative information about the processes occurring in the reactor during film growth. The major organic thermolysis products found for **1**, isobutene and HS^{t}Bu (eq 1), suggest that β-hydrogen elimination followed by proton transfer from hydrosulfide to a thiolato ligand and subsequent mercaptan dissociation are the principal pyrolysis pathways (eqs 3 and 4). The organic thermolysis products are the same as those found by Girolami and co-workers for the homoleptic *tert*-butylthiolates M(S^{t}Bu)$_4$ (M = Ti, Mo).[32] However, in the present case of **1**, only traces of H_2S are detected, versus HS^{t}Bu/H_2S ratios of 3.3:1 (Mo(S^{t}Bu)$_4$) and 10:1 (Ti(S^{t}Bu)$_4$), respectively, showing that alternative proton transfer from one hydrosulfide to another is less prevalent. Similar to our findings, Pickett et al. reported that the pyrolysis of d^{10} ZnS *single-source* precursor [MeZnS^{t}Bu]$_5$ under a flow of argon effects disproportionation to $ZnMe_2$ and Zn(S^{t}Bu)$_2$, the latter forming HS^{t}Bu and isobutene as the major organic products.[33] These results differ from the solid-state vacuum pyrolysis studies of M(S^{t}Bu)$_2$ (M = Zn, Cd, Pb) by Rees et al., which detected mainly $S_2{}^tBu_2$ as the organic pyrolysis product.[34] The disulfide was assigned as a secondary pyrolysis product of initially formed S^{t}Bu$_2$, but it remained unclear if the sulfide was a reaction intermediate itself, for example, from addition of *tert*-butylthiol to isobutene. In the case of **1**, the minor amounts of bis-*tert*-butyldisulfide and isobutane detected suggest that radical pathways (eqs 5−7) are unimportant, making it most unlikely that S^{t}Bu$_2$ arises from recombination of isobutyl and *tert*-butylsulfanyl radicals. Furthermore, the absence of the anti-Markownikoff product ^{t}BuS^{i}Bu indicates that S^{t}Bu$_2$ is not formed by gas-phase reaction of *tert*-butylsulfanyl radicals with isobutene.[35] Instead, Markownikoff addition of HS^{t}Bu to isobutene is well-known to be faciliated by Brønstedt and Lewis acid catalysts, and copper-centered addition therefore seems to be the most likely pathway for S^{t}Bu$_2$ formation (eq 8).[36] We proposed the same pathway for precursor $Cu_7(S^tBu)_4(hfa)_3(PMe_3)_3$ with Lewis acidic Cu(hfa) building blocks in the cluster core, with no evidence for radical process products (isobutane, di-*tert*-butyldisulfide) being found.[12] Although radical reactions are of minor relevance to the overall pyrolysis process, they may be important for the electronic properties of the materials grown because homolytic C−S bond cleavage reactions (eq 5) could account for $Cu^I \rightarrow Cu^{II}$ partial oxidation, consistent with the observed intrinsic *p*-type doping of α-Cu_2S thin films.[31]

As shown by TGA, the majority of the phosphine ligands dissociate prior to C−S cleavage, leading to considerably lower local phosphine concentrations during thiolate decomposition. However, the phosphine dissociation and C−S bond activation regions clearly overlap in the TGA, and the thermolysis of **2a**/**b** and **3** is complete at somewhat higher temperatures than for parent **1**, indicating the presence of PR_3 upon onset of thiolate pyrolysis. Nevertheless, we do not find phosphine sulfides $R_3P{=}S$ (R = Me, Et) in the trapping experiments although the standard heat of formation of α-Cu_2S at 300 K ($\Delta_f H^0 = -84$ kJ·mol^{-1}) is considerably smaller than the heat of oxidation of trialkylphosphines PR_3 (R = Me, ^{n}Bu) to phosphinesulfides by elemental sulfur ($\Delta_r H^0 = -117$ kJ·mol^{-1}).[37,38] Furthermore, pyrolysis of **3** gives identical decomposition products at very similar temperatures despite the greater P/S ratio. Finally, Cu_2S AACVD film growth experiments with precursor **2a** and additional PMe_3 (Cu/P ratio: 1) yielded the same Cu_2S films with respect to microstructural and electronic properties, despite the fact that small Cu_xS stoichiometry changes are known to substantially alter the free carrier concentration.[31] Therefore, it remains unclear if the reduction of cuprous sulfide by the trialkylphosphine ligands is only kinetically hindered or actually becomes thermodynamically unfavorable at elevated temperatures.[39] As an example, $\Delta_f H^0$ of FeS (Trolite = −102 kJ·mol^{-1}) at room temperature is well above $\Delta_r H^0$ of phosphine oxidation by sulfur.[40] However, metallic Fe is known to be an efficient $^nBu_3P{=}S$ desulfurization agent at temperatures around 300 °C.[41]

Conclusions

The rich cluster chemistry of polymeric **1** with phosphines was examined in the solid state and for the first time in

(31) Schneider, S; Ireland, J. R.; Hersam, M. C.; Marks, T. J. *Chem. Mater.* **2007**, *19*, 2780.
(32) Cheon, J.; Gozum, J. E.; Girolami, G. S. *Chem. Mater.* **1997**, *9*, 1847.
(33) Pickett, N. L.; Lawson, S.; Thomas, W. G.; Riddell, F. G.; Foster, D. F.; Cole-Hamilton, D. J.; Fryer, J. R. *J. Mater. Chem.* **1998**, *8*, 2769.
(34) (a) Kräuter, G.; Favreau, P.; Rees, W. S., Jr. *Chem. Mater.* **1994**, *6*, 543. (b) Rees, W. S., Jr.; Kräuter, G. *J. Mater. Res.* **1996**, *11*, 3005.
(35) Griesbaum, K. *Angew. Chem., Int. Ed. Engl.* **1970**, *9*, 273.
(36) (a) Posner, T. *Ber. Dtsch. Chem. Ges.* **1905**, *38*, 646. (b) Screttas, C. G.; Micha-Screttas, M. *J. Org. Chem.* **1979**, *44*, 713. (c) Kondo, T.; Mitsudo, T. *Chem. Rev.* **2000**, *100*, 3205. (d) Kanagasabapathy, S.; Sudalai, A.; Benicewicz, B. C. *Tetrahedron Lett.* **2001**, *42*, 3791.
(37) Brooks, A. A. *J. Am. Chem. Soc.* **1953**, *75*, 2464.
(38) (a) Chernick, C. L.; Pedley, J. B.; Skinner, H. A. *J. Chem Soc.* **1957**, 1851. (b) Capps, K. B.; Wixmerten, B.; Bauer, A.; Hoff, C. D. *Inorg. Chem.* **1998**, *37*, 2861.
(39) High temperature thermodynamic data for phosphine oxidation by sulfur has not been reported to our knowledge.
(40) Chase, M. W. *NIST-JANAF Thermochemical Tables*, 4th ed.; Journal of Physical and Chemical Reference Data Monograph 9; American Institute of Physics: Woodbury, NY, 1998; Part II.
(41) Maier, L. *Helv. Chim. Acta* **1964**, *47*, 2137.

Scheme 4. Thermolysis Sequences for $(CuS^tBu)_4(PR_3)_2$ Complexes in the Solid State (R = Me (2a), Et (2b))

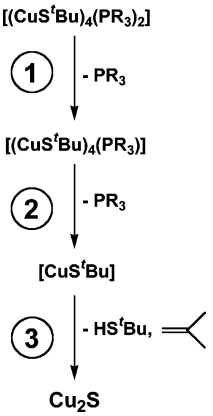

solution. The latter is of particular relevance to recently emphasized solution-based film growth techniques, such as AACVD.[10] Both trimethyl- and triethylphosphine compounds **2a** and **2b** form 1:2 adducts with **1** which are isostructural with $(CuS^tBu)_4(PPh_3)_2$. While they are configurationally stable in toluene, a marked difference between the phosphine ligands is observed in more polar solvents such as CH_2Cl_2 or THF, with **2a** engaging in rapid ligand exchange equilibria. The formation of ion pair **3** has been identified as the driving force for this solution behavior while the steric bulk of PEt_3 is too great to stabilize the analogous $Cu(PEt_3)_4^+$ cation. Starting from the dominant structural motif for **2a**, **2b**, **3**, and **5** in the solid state, mechanisms for the facile interconversion of the thiolate clusters are proposed based on a flexible Cu_4S_4 eight-membered ring with the Cu atoms arrayed in a single plane.

The clean thermolysis to α-Cu_2S renders clusters **1**−**3** excellent *single-source* precursors. A detailed description of their use in high-quality chalcocite thin film growth can be found in the accompanying paper.[31] Facile phosphine ligand cleavage makes precursors **2** and **3** amply soluble sources of polymeric **1** with ideal thermal properties as precursors for aerosol-based Cu_2S growth. Subsequent β-H-elimination from the *tert*-butyl substituent and HS^tBu dissociation after H^+ transfer are plausibly the dominant C−S and Cu−S bond cleavage reactions (Scheme 4). Radical processes play only a minor role in the overall pyrolysis but can account for slight deviations from ideal Cu_2S stoichiometry.

As a result of their strong π-basicity, thiolato ligands are ideal building blocks for the design of functional multimetallic clusters, for example, *single-source* precursors for ternary and quaternary materials. In the future we plan to further examine the exploitation of thiolato clusters for the growth of complex cuprous sulfide materials for optoelectronic applications.

Acknowledgment. We thank the NSF (CMS-0510895), the NSF MRSEC program (DMR-0076097), and NREL (XAT-5-33636-02) for financial support of this research and C. L. Stern for single-crystal X-ray data acquisition. S.S. thanks the DFG for a postdoctoral fellowship under the Emmy-Noether Programm.

Supporting Information Available: Mass spectrometric and low-temperature NMR spectroscopic data (PDF) and X-ray crystallographic files (CIF) of **2a**, **2b**, **3**, **4**, and **5**. This material is available free of charge via the Internet at http://pubs.acs.org.

CM0700504